

Resonant photoemission at the absorption edge of Mn and Ti and electronic structure of $1T\text{-Mn}_x\text{TiSe}_2$

M.V. Yablonskikh¹, Y.M. Yarmoshenko², A.S. Skvarin², N.A. Skorikov² and A.N. Titov^{2,3}

¹ Sincrotrone Trieste SCpA, Basovizza I-34012, Italy

² Institute of Metal Physics, Russian Academy of Sciences-Ural Division, 620041 Yekaterinburg, Russia

³ Ural State University, pr. Lenina 51, Yekaterinburg, 620089 Russia

Received: date / Revised version: date

Abstract. Resonant valence-band X-ray Photoemission Spectra (RXPS) excited at $2p_{3/2}$ core level energies, $2p_{3/2}$ X-ray Photoelectron Spectra (XPS) and $L_{3,2}$ X-ray Absorption Spectra (XAS) of Ti and Mn in single crystals $1T\text{-Mn}_x\text{TiSe}_2$ ($x=0.1, 0.2$) were studied for the first time. The ionic-covalent character of bonds formed by Mn atoms with the neighboring Se atoms in the octahedral coordination is established. Atomic multiplet calculations of Ti and Mn $L_{3,2}$ XAS considering Ti in the state $4+$ and Mn in the state $2+$ are found to be in a good agreement with experiment. Performed electronic structure calculations of the $\text{Mn}_{1/8}\text{TiSe}_2$ compound are also in a good agreement with experimental RXPS data. RXPS of the valence band exhibit narrow Ti 3d and Mn 3d bands which are localized immediately under the Fermi level. From the theoretical calculations the localization of the Ti 3d and Mn 3d states in the Brillouin zone of the crystal was determined.

PACS. 74.25.Jb Electronic structure (1082) – 31.10.+z Theory of electronic structure, electronic transitions, and chemical binding (276) – 71.20.Be Transition metals and alloys – 78.70.Dm X-ray absorption spectra – 79.60.-i Photoemission and photoelectron spectra

1 Introduction

Layered dichalcogenides of Ti intercalated with transition metals Me_xTiZ_2 (Me-transition metal, $Z = \text{S, Se, Te}$) show a promise in creation of monoatomic layers of magnetic

metals with a given density. These layers are separated by nonmagnetic packets of the TiZ_2 matrix. Such substances are natural analogs of nanostructures. The systematic studies [1,2,3] of chemical bonding in the Me_xTiZ_2 ,

compounds revealed that hybridization of 3d states of an interstitial metal atom and its nearest neighborhood is pure covalent in its origin. The covalence of the chemical bonding results in the shrink of the lattice in the direction aligned with the normal to the basis plane [4], decrease in conductivity [2], formation of narrow and dispersion-less zones in the vicinity of the Fermi level [5,6], and suppression of the magnetic moment of interstitial atoms [7] due to delocalization of their 3d electrons. The only exception from this group of materials is the Mn_xTiSe₂ system which, upon intercalation, exhibits an increase in the interlayer spacing, growth of conductivity [8], and anomalously high (by the order of magnitude) increment of the Pauli contribution to the magnetic susceptibility in comparison with the other intercalated metals [9].

In our work all experimental data were taken from single crystals of 1T-Mn_xTiSe₂ ($x = 0.1; 0.2$). To understand the origin of the anomalous behavior of the Mn-TiSe₂ system, XPS of the Ti 2p and Mn 2p core levels, L_{3,2} XAS of Ti and Mn, and valence band RXPS excited across the L₃ edges have been investigated.

2 Experiment and calculations

Single crystals of Mn_xTiSe₂ were grown by the gas-transport reaction technique with I₂ as a gas-carrier in evacuated quartz ampoules from a polycrystalline phase. Crystals have a form of thin plates of about $2 \times 2 \times 0.05$ mm² in size. The chemical composition was determined by X-ray fluorescence analysis using a JEOL-733 spectrometer. The crystal structure the same as reported on earlier [7]. The

analysis showed the preservation of composition of the initial phase in the course of growing single crystals¹. In Fig. 1 the fragment of the crystal structure and the Brillouin zone of the compound 1T-Mn_xTiSe₂ are shown.

All the measurements were performed at BACH beam-line [10] of the Elettra synchrotron Facility. Photoelectron Spectra were taken using an VSW 150 photoelectron analyzer with the acceptance angle of 8 degrees. X-ray absorption data were measured in the Total Electron Yield (TEY) mode. The sample was cleaved in-situ in a vacuum lower than $1 \cdot 10^{-9}$ torr [$3-5 \cdot 10^{-10}$]. XPS of the C 1s, O 1s and Ti 2p core levels were measured from time to time to check for contamination of the surface during the measurements. The intensity of carbon and oxygen 1s peaks in survey spectra was extremely low and the shape of Ti 2p XPS remained unchanged during the measurement. The absence of the titanium oxide like satellite peaks in Ti 2p XPS serves as an indication of the absence of the possible oxidation of the sample surface. The angle between the incoming beam and the normal to the basis plane of the sample was 60 degrees. The normal to the sample was parallel to the c-axis which was aligned with the axis of the analyzer. Both the c-axis [001] of the sample and the polarization of the incident X-ray were in horizontal plane.

The energy resolution of the monochromator i.e, resolution of the absorption spectra (E_{mono}) at the Ti 2p edge was 0.12 eV, the photoelectron analyzer resolution E_{pa} was set to 0.147 eV, which results in the total en-

¹ the details of the crystal structure investigations will be published elsewhere

ergy resolution $E_{tot}=0.19$ eV. For the Mn 2p edge, $E_{mono}=0.14$ eV and $E_{pa}=0.220$ eV, which results in $E_{tot}=0.26$ eV. The RXPS of the valence band measured at excitation energies selected near the Ti 2p edge have a total resolution of 0.18 eV with $E_{mono}=0.11$ eV and $E_{pa}=0.18$ eV. The same parameters for the case of Mn 2p excitations are $E_{mono}=0.15$ eV, $E_{pa}=0.15$ eV, $E_{tot}=0.21$ eV. The binding and monochromator energies were calibrated through the binding energy of Au 4f_{3/2} level and through the Fermi edge measurements.

All band structure calculations were performed using the full-potential augmented plane-wave method as implemented in WIEN2k code [11]. To account for the exchange-correlation potential we employed the gradient approximation [12] in the Perdew-Burke-Ernzerhof variant. The Brillouin zone integrations were performed with a $7 \times 7 \times 3$ special k-point grid and $R_{MT}^{min} \cdot K_{max}=7$ (the product of the smallest of the atomic sphere radii R_{MT} and the plane wave cutoff parameter K_{max}) was used for the expansion of the basis set. The experimentally determined lattice parameters of Mn_{0.145}TiSe₂ ($a_0=3.5770 \text{ \AA}$, $c_0=6.1645 \text{ \AA}$) were taken. The spheres radii were chosen $R_{Mn}=2.46$, $R_{Ti}=2.5$, $R_{Se}=2.19$ a.u. so that the spheres be nearly mutually touching. To account for intercalation TiSe₂ by Mn atoms we constructed a $2a_0 \times 2a_0 \times 2c_0$ supercell in which for one of the non-equivalent selenium atoms the z -parameter was chosen as in pristine TiSe₂ whereas for the second Se atom (placed near the Mn layer) the experimentally determined z -parameter was used. The resulting

unit cell has the same symmetry as the initial unit cell of the TiSe₂: space group P-3m1 (164), see also Fig. 1.

The atomic multiplet calculations of L_{3,2} absorption spectra of Ti⁴⁺ and Mn²⁺ in the octahedral neighborhood (pore) were performed with the use of the program from [13]. In the calculations of the Ti L_{3,2} XAS the best agreement with the experiment is observed with the following specified parameters: Slater integrals are decreased to 75% the calculated value, parameter of splitting in the crystal field $10Dq$ equal to 1.2 eV, the charge transfer parameter Δ was equal to 3 eV. In the Mn L_{3,2} XAS for Mn_{0.2}TiSe₂ the crystal field splitting was $10Dq=0$ eV, Slater integrals made up 100% of the calculated value, the charge transfer parameter Δ was equal to 3 eV. As was shown earlier [8], for Mn concentrations up to $x=0.25$ the compound Mn_xTiSe₂ can be treated as pure two-dimensional. Therefore, when discussing the experimental results we use a two-dimensional model of the Me_xTiZ₂ compounds. With no allowance for possible ordering in the Me sublattice, the crystal structure of these compounds is hexagonal.

3 Experiment, Theory and Discussion

3.1 XPS

The results of measurements of Ti 2p, Se 3d spectra are shown in Fig. 2. The binding energy (E_b) of the Ti 2p_{3/2} level for the compound TiSe₂ is equal to $E_b=455.0$ eV. For the intercalated compound the shift of the binding energy of the spectral maxima in the Ti 2p and Se 3d lines is

observed. The shift magnitude grows with the increase of Mn concentration. The Ti 2*p* lines of the multiplet in the intercalated compound are essentially broadened in comparison with that from the pure compound [2]. This can be accounted for summing up the spectral contributions from titanium atoms occupying two crystallographically nonequivalent positions in the lattice, Ti1 and Ti2. In the intercalated compound the nearest neighborhood of atoms Ti2 is identical to that in the matrix of TiSe₂, with Mn atoms occupying sites in the second coordination shell of Ti1 (Fig. 1). Se atoms are to be treated in the same manner.

Therefore, we take into account these contributions when calculating electronic structure and interpreting the experimental results. After subtracting the background, the Ti 2*p* and Se 3*d* spectra were fitted with two components (Fig. 2) under assumption that the main contribution to the spectra comes from lines Ti and Se in the matrix TiSe₂. Although such fitting does not reproduce exactly the contribution v.s. Mn concentration behavior, a correlation between the weighted components of the spectra and the content of intercalated Mn is observed. Besides, it is evident that the positive shift of the binding energy $\Delta E=1$ eV comes from the atomic spectra of the first kind. Such description clearly represents how even small amount of Mn atoms introduced exert a remarkable effect on the formation of electronic structure in the compound under consideration.

Mn 2*p* spectra present the most meaningful information on the state of Mn atoms in the lattice, which de-

termine the physical properties of the material. Mostly due to low concentration of Mn we were able to measure Mn 2*p* core levels only for the concentration $x=0.2$. There are two important observations: first, the Mn 2*p* spectrum shows up a satellite structure at the energy which is lower than the main lines by 6 eV and, second, the line shape is very similar to that observed for MnO [14]. Similar high-energy satellites are also observed in oxides of other transition metals. The physical explanation of the appearance of high-energy satellites in the Mn 2*p* XPS is based on the model of the ground state in the approximation [15, 16, 17]

$$\varphi_g = \alpha|d^5 + \beta|d^6 + \gamma|d^7\underline{L}^2 \quad (1)$$

where L denotes the ligand hole in the Se 4*p* states; α , β and γ are the amplitudes of the corresponding states. In the final state the Coulomb interaction between the hole \underline{c} and Mn 3*d* electrons arises. As a result of this interaction, the levels of the final states $\underline{c}d^5$ and $\underline{c}d^6$ come closer to each other.

It was established that MnO is not a pure ionic compound, since the ground state is significantly contributed to by configuration $d^6\underline{L}$ [14]. Owing to the coincidence of the shape and position of the satellites, we can apply the conclusions made for MnO to the case of our compound as well. In Mn_{0.2}TiSe₂ the chemical bond of Mn atom with the neighbor atoms displays the similar character. Electrons are transferred from the manganese ions in the state Mn²⁺ to the conduction band formed by the Ti 3*d* states. It should be noted that in the compounds intercalated with other transition metals the charge to be

transferred is negligibly small, which is quite decisive in distinguishing compounds with Mn from dichalcogenides intercalated with other transition metals.

3.2 XAS

Let us discuss the Ti L_{3,2} and Mn L_{3,2} XAS (4) measured under the same experimental conditions as XPS. The Ti L_{3,2} XAS differ by shape and energy position from the spectrum of pure TiSe₂ which we reported on earlier [18]. The main reason for this possibly is that upon introduction of Mn atoms in the Van der Waals spacial gap of the TiSe₂ matrix there takes place a deformation of chalcogenic surrounding of Ti atoms and the charge transfer from Mn into the conduction band. The amplitude of deformation is featured by the parameter $\varepsilon = (2zc_0)/a_0$, where c_0 and a_0 are the lattice constants, and z is the coordinate of Se atom in the unit cell. The intercalation of Mn to the composition Mn_{0.2}TiSe₂ results in the change ε from 0.8655 in TiSe₂ to 0.8792 ($\Delta\varepsilon = 0.0137$). It has to be noted that the amplitude of deformation $\Delta\varepsilon$ has a quite large magnitude for case of Mn_xTiSe₂ in comparison with the cases of intercalation of other metals. For example, introduction of Cr results in the quantity $\varepsilon = 0.8651$ ($\Delta\varepsilon = 0.0004$), which is by two orders of magnitude smaller than for Mn_{0.2}TiSe₂. Such deformation should enhance the splitting of the lower unfilled Ti 3d_{z²}-orbital from the rest Ti 3d states, increase the binding energy of Ti d_{z²} orbital [19], and, consequently, result in the partial filling of the electronic states in the vicinity of the Fermi level.

The calculation results of Ti L_{3,2} XAS in the oxidation state of 4+ (Fig. 3) are in a good agreement with experimental data. The absorption spectrum of titanium in Mn_{0.2}TiSe₂, similar to photoelectron spectrum Ti 2p, is a superposition of weighted contributions from Ti1 and Ti2. In the calculated spectrum the main maxima A and B correspond to the mass centers of the e_g and t_{2g} orbitals, though they are strongly intermixed. Splitting into (anti-bonding) t_{2g} and e_g orbitals of the Ti L₃ and Ti L₂ components of the multiplet in the crystal field is equal to 1.2 eV (Fig. 4) unlike 1.8 eV in the case of TiSe₂. However, the calculated absorption spectrum does not reproduce the C maximum which is observed in the experimental one due to the model limitations discussed in the Sec. 2 and further. However, from comparison of the experimental data taken for TiSe₂ [18] we can assume that the energy position of the C maximum is due to the contribution of Ti2 atoms.

The calculated absorption spectrum of Mn in the oxidation state 2+ reproduces the shape and energy position of the main spectral maxima much better than that for Ti case. The energy splitting of t_{2g} and e_g orbitals is absent.

3.3 RXPS

Photoemission of *d* electrons from 3d metals and their compounds is strongly enhanced if the energy of the incident photon exceeds the binding energy of the core level upon excitation of *np* electrons ($n=2,3$) to an unfilled 3d state, resulting in a resonant emission [20,21,22,23, 24,25]. This effect is interpreted as a result of a consis-

tent process under which an np electron in the initial state first is excited to an empty $3d$ level, thus forming an intermediate bound state ($np, 3d$). Because of autoionization this intermediate state can transform into a final state identical to that resulting from the direct photoemission. The resonance of $3d$ electrons of Ti and Mn takes place upon interference of the direct channel of photoemission ($np^6 3d^n + h\nu \rightarrow np^6 ed^{n-1} e_f$) with the successive decay of the excited state of the Coster-Kronig type ($np^6 ed^{n+1} + h\nu \rightarrow np^5 3d^{n+1} \rightarrow np^6 3d^{n-1} e_f$). The resonance profile of the spectrum in the valence band is superimposed on the intense peaks of the Auger L_{2,3}M_{4,5}M_{4,5} line. They arise at the excitation energies near and above at the $2p$ edge of absorption and may essentially overlap with the valence band peaks.

The Ti $2p_{3/2}$ and Mn $2p_{3/2}$ RXPS of the valence band are shown in Fig.5. In the normal mode of the Resonance Raman Auger Spectra (RRAS)[26] the position of the Auger signal on the binding energy scale does not change with the excitation energy until the latter reaches the Ti L₃. The situation is similar to that studied in detail for some $3d$ metals in [24]. Upon the subsequent increase in the excitation energy, a standard Auger L₃VV spectrum that possesses a constant kinetic energy is registered. The spectra are overlapped with an Auger peak changing its position in the binding energy scale to up to 10 eV following the increase of the photon energy. In our experiments the appearance of the crossover in the Ti $2p_{3/2}$ valence band RXPS coincides with the binding energy of the spectral maximum (point **f**) in the Ti L₃ absorption

spectrum. Mn $2p_{3/2}$ RXPS behave themselves in the similar manner. Important is the appearance of two peaks in the vicinity of the Fermi energy: Ti_{*d*} in the valence band of Ti $2p$ RXPS and Mn_{*d*} in the Mn $2p$ RXPS.

The intensity of Mn_{*d*} peak is the smallest when comparing to the rest of the valence band peaks, but maximal for the excitation energy corresponding to peak maxima **f**) in Mn L₃ absorption spectrum. Per contra, the intensity of Ti_{*d*} peak is higher relatively to that of the rest of the manifold but also reaching its maximum for the photon energy **i**) of Ti L₃ absorption peak. Taking in account the small concentration of Mn atoms relatively to that of Ti (1-2 to 10) it is expected that the intensity of Mn_{*d*} peak will be much smaller than that of Ti_{*d*} peak even for resonant excitation. Note that the CIS spectra presented in Fig 6 include all the peculiarities inherent from the L₃ XAS of titanium and manganese. That tendency let us conclude about the localized nature of Mn $3d$ and Ti $3d$ states in the vicinity of the Fermi energy.

Before we compare density of states and wavefunction calculations with experimental data, it is important to mention all reasons which explain the Ti_{*d*} to the rest of manifold peak ratio to be larger than that of Mn_{*d*} to the rest of manifold. At energies of excitation in the ranges of $2p$ resonance of Ti and Mn the mean free path of inelastically scattered electrons does not exceed 10 Å [24], whereas the photoionization cross-section for Ti $3d$ is approximately 3-4 times as large as that for Mn $3d$. Minding the crystal structure of the compound (Fig. 1), one should expect an enhancement of the output for Ti $3d$ electrons

in comparison with Mn 3d electrons (the nearest to the crystal surface Van der Waals spatial gap containing Mn atoms is located at a distance of 12 Å). Besides, the crystal surface (the cleavage surface) loses part of Mn atoms, when some layer is chipped. Therefore, the sample layer under examination and the corresponding spectra contain not all elements of the crystal symmetry, unlike the theoretical model. Moreover, in the experiment the *c* axis is parallel to the analyzers axis. According to the theoretical calculations of $E(\mathbf{k})$ in the vicinity of this point immediately under the Fermi level, the Ti 3d states prevail. (Fig. 7). The Mn 3d states are localized mainly near the points K and M of the Brillouin zone (7). In our experimental geometry we would expect the most favorable conditions for the photoelectron emission from the vicinity of point Γ of the Brillouin zone, despite of the magnitude of the excitation energy which is high enough to cover the first Brillouin zone for Ti 2p and Mn 2p excitations. Therefore, we assume that the photoemission intensity is determined by the direction of vector \mathbf{k} of the emitted electron in the Brillouin zone. However, for the selected excitation energies the angular resolution of the analyzer does not allow to distinguishing the points of high symmetry. We would also assume that upon excitation with the energy corresponding to point \mathbf{f}) in the absorption spectrum of Ti in Fig. 5, mainly the t_{2g} states become excited, whereas on coming to point \mathbf{i}) the e_g states started to contribute. The bottom line is that for both Mn and Ti 2p_{3/2} RXPS peaks Mn_d and Ti_d represent a mixture of the t_{2g} and e_g states.

4 Conclusion

Atoms of titanium and manganese are shown to possess the oxidation degree +4 and +2, and, consequently, in the case of Mn, the ionic component of the chemical bond in the octahedral neighborhood identical to that of Ti prevails. These results are confirmed by the atomic multiplet calculations of Ti and Mn XAS. In the spectrum of Mn 2p XPS, satellites have been registered at a distance of 6 eV from the main lines, which evidences the partly covalent chemical bonding. The band structure calculation for the compound 1T-Mn_{0.125}TiSe₂ have been performed which present a good agreement of the results with the experimental data. In the XPS of the valence band, on reaching the 2p resonance for Ti and Mn, narrow d bands of mixed orbital symmetry which are localized immediately under the Fermi level are observed.

From the theoretical calculations of $E(\mathbf{k})$ it is established that under the Fermi level the Ti 3d states are localized in the vicinity of point Γ of the Brillouin zone of the crystal. The Mn 3d states are localized along the direction M- Γ -K.

5 Acknowledgment

We acknowledge the financial support of the RFBR, grant N 09-03-00053 and F. de Groot for the opportunity to use his XAS code. Michele Zacchigna for fruitful scientific discussion and Federica Bondino for technical assistance at the beamline.

References

1. A.V. Postnikov, M. Neumann, S. Plogmann, Y.M. Yarmoshenko, A.N. Titov, A.V. Kuranov, *Comp. Mat. Science* **17**(2-4), 450 (2000)
2. A.N. Titov, A.V. Kuranov, V.G. Pleschev, Y.M. Yarmoshenko, M.V. Yablonskikh, A.V. Postnikov, S. Plogmann, M. Neumann, A. Ezhov, E. Kurmaev, *Phys. Rev. B* **63**(3), 035106 (2001)
3. A.N. Titov, S.G. Titova, M. Neumann, V.A. Pleschov, Y. M.Yarmoshenko, L.S. Krasavin, A.V. Kuranov, *Mol. Cryst. Liq. Cryst.* **311**, 161 (1998)
4. A.N. Titov, A.V. Dolgoshein, I.K. Bdikin, S.G. Titova, *Sol. State Phys.* **42**(9), 1610 (2000)
5. T.V. Kuznetsova, A.N. Titov, Y.M. Yarmoshenko, E.Z. Kurmaev, A.V. Postnikov, V.G. Pleschev, B. Eltner, G. Nicolay, D. Ehm, S. Schmidt et al., *Phys. Rev. B* **72**(8), 085418 (2005)
6. X.Y. Cui, H. Negishi, S.G. Titova, K. Shimada, A. Ohnishi, M. Higashiguchi, Y. Miura, S. Hino, A. Jahir, A. Titov et al., *Phys. Rev. B* **73**(8), 1 (2006)
7. A.N. Titov, Y.M. Yarmoshenko, M. Neumann, V.G. Pleschov, S.G. Titova, *Sol. State. Phys.* **46**(9), 1681 (2004)
8. V.I. Maksimov, N.V. Baranov, V.G. Pleschov, K. Inoue, J. *Alloys and Comp* **384**(1-2), 33 (2004)
9. Y. Tazuke, T. Takeyama, *J. Phys. Soc. Jap.* **66**(3), 827 (1997)
10. M. Zangrando, M. Finazzi, G. Paolucci, G. Comelli, B. Di-
viacco, R. Walker, D. Cocco, F. Parmigiani, *Rev. Sci. Instr.* **72**(2), 1313 (2001)
11. P. Blaha, K. Schwarz, G.K.H. Madsen, D. Kvasnicka, J. Luitz, An augmented plane wave + local orbitals program for calculating crystal properties
12. J.P. Perdew, K. Burke, M. Ernzerhof, *Phys. Rev. Lett.* **77**(18), 3865 (2010)
13. E. Stavitski, F.D. Groot., *Micron* (2010)
14. J. van Elp, R.H. Potze, H. Eskes, R. Berger, G.A. Sawatzky, *Phys. Rev. B* **44**(4), 1530 (1991)
15. J. Ghijsen, L.H. Tjeng, J. van Elp, H. Eskes, J. Westerink, G.A. Sawatzky, M.T. Czyzyk, *Phys. Rev. B* **38**(16), 11322 (1988)
16. G. van der Laan, C. Westra, C. Haas, G.A. Sawatzky, *Phys. Rev. B* **23**(9), 4369 (1981)
17. J. Zaanen, C. Westra, G.A. Sawatzky, *Phys. Rev. B* **33**(12), 8061 (1986)
18. A.N. Titov, Y.M. Yarmoshenko, A. Zimina, M. Yablonskikh, A. Postnikov, S. Eisebitt, *Sol. St. Phys.* **50**(6), 1186 (2008)
19. S. Bayliss, W. Liang, *J. Phys. C: Sol. State Phys* **17**(12), 2193 (1984)
20. J.W. Allen, Synchrotron Radiation Research, Vol. 25 (Plenum Press, N.Y., 1992)
21. A. Kay, E. Arenholz, S. Mun, F.G.D. Abajo, C.S. Fadley, R. Denecke, Z. Hussain, M.A.V. Hove, *Science* **281**(5377), 679 (1998)
22. Special issue on resonant inelastic soft x-ray scattering, See *Appl. Phys. A: Mater. Sci. Process* **65** (1997)
23. N. Mårtensson, M. Weinelt, O. Karis, M. Magnuson, N. Wassdahl, A. Nilsson, J. Stöhr, M. Samant, *Appl. Phys A: Materials Science and Processing* **65**(2), 159 (1997)
24. G.B. Armen, H. Wang, *Phys. Rev. A* **51**(2), 1241 (1995)

25. C.J. Powell, A. Jablonski, J. Phys. Chem. Ref. Data **28**(1),
19 (1999)
26. S. Hüfner, S. Yang, B. Mun, C. Fadley, J. Schäfer,
E. Rotenberg, S. Kevan, Phys. Rev. B **61**(19), 12582 (2000)

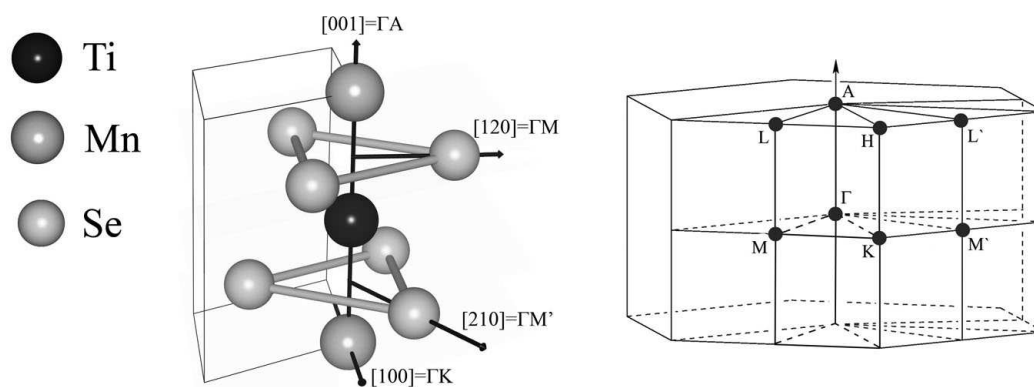


Fig. 1. A fragment of the Mn_{0.2}TiSe₂ crystal and Brillouin zone for the 1T-TiSe₂ compound. Γ -A direction in the Brillouin zone corresponds to the direction of the crystallographic *c*-axis perpendicular to the basic plane of the crystal in the direct space ([001] direction).

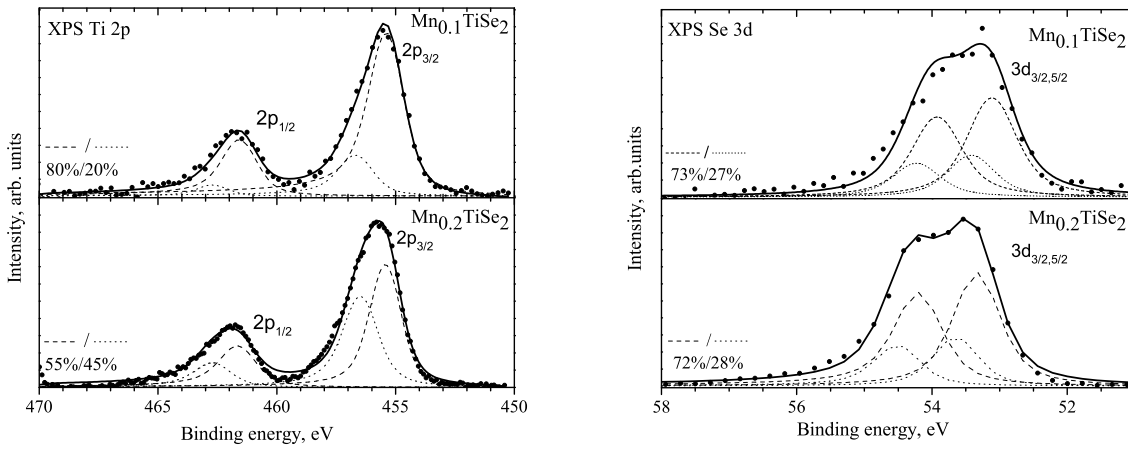


Fig. 2. XPS of Ti 2p and Se 3d core levels in Mn_xTiSe₂ ($x=0.1$ and 0.2) and their convolution data are presented. In the spectra of Se 3d level the main change in the coordination of the TiSe₆ clusters consists in the line shift. The ratio of the spectral contributions Ti₂/Ti₁ (—/— —) from different crystallographic positions of Se atoms when compared between the cases of $x=0.1$ and $x=0.2$ virtually does not change for Se XPS per contra to that for Ti XPS.

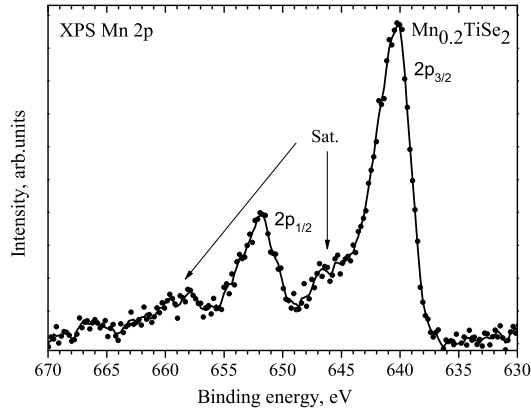


Fig. 3. Photoelectron spectrum of Mn 2p in Mn_{0.2}TiSe₂. Positions of the satellites are marked with the label "Sat.".

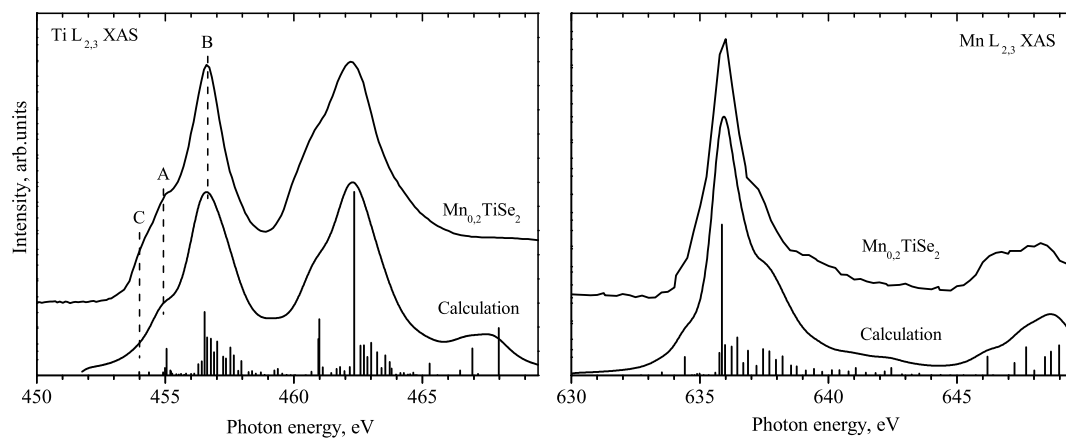


Fig. 4. Experimental and calculated Ti L_{3,2} and MnL_{3,2} absorption spectra for the sample Mn_{0.2}TiSe₂

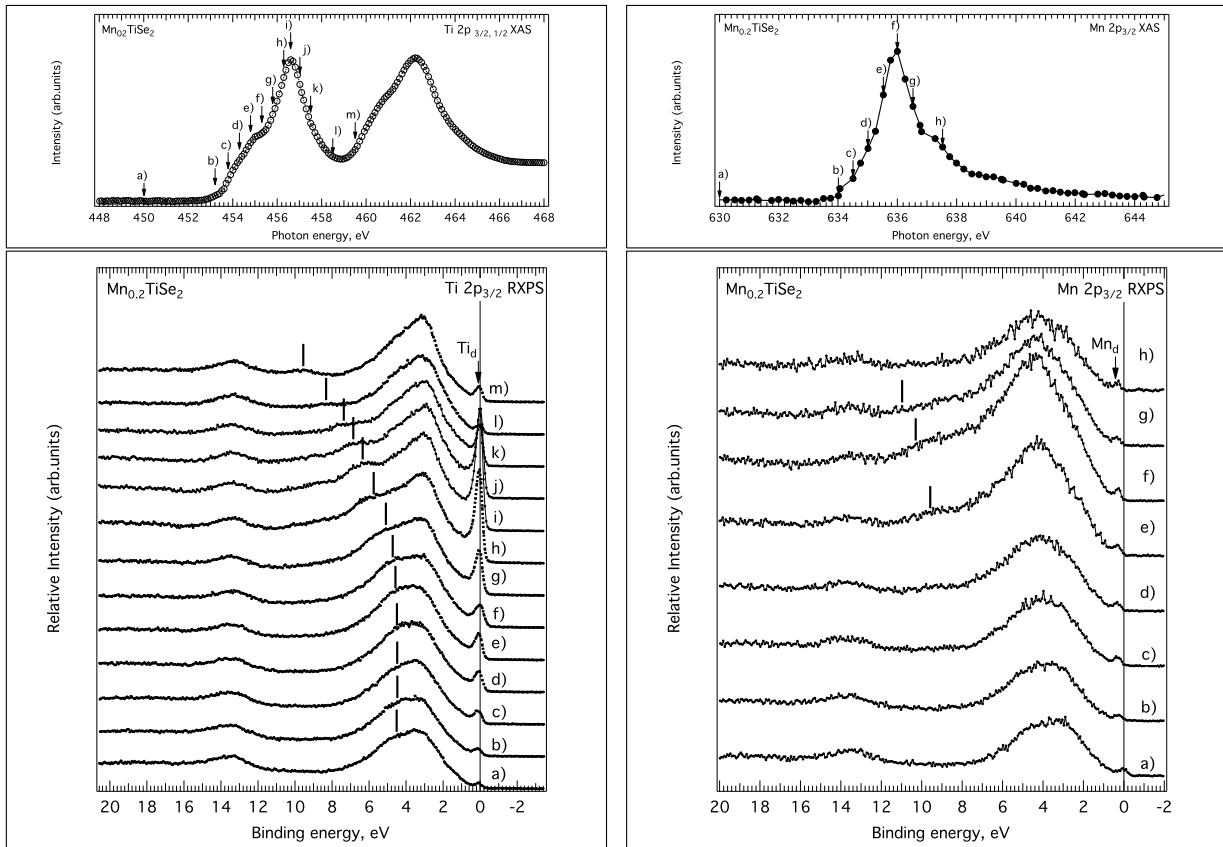


Fig. 5. Ti and Mn $2p_{3/2}$ RXPS are at the left and the right frames. In the upper part of the left frame the Ti $L_{3,2}$ absorption spectrum is given denoted as Ti $2p$ XAS. Photoelectron spectra of the valence band in $Mn_{0.2}TiSe_2$ acquired at the $2p_{3/2}$ resonance of Ti are shown in the lower part of the frame. Labels from a) to m) at the corresponding photoelectron spectra (bottom) mark the excitation energy taken from the absorption spectrum. Dashes show the positions of the Auger peaks depending on the excitation energy. The peak with the binding energy 13.5 eV corresponds to the Se $4s$ band. The meaning of similar labels in the right frame is the same as for the left frame

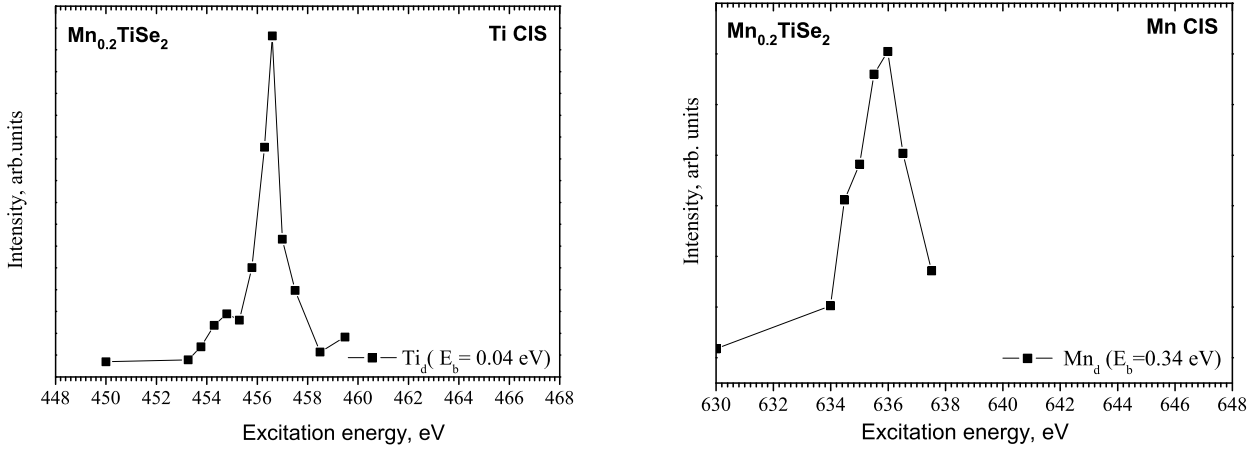


Fig. 6. Ti and Mn Constant Intensity Spectra (CIS) of the photoemission peaks Ti_d and Mn_d taken from the corresponding RXPS.

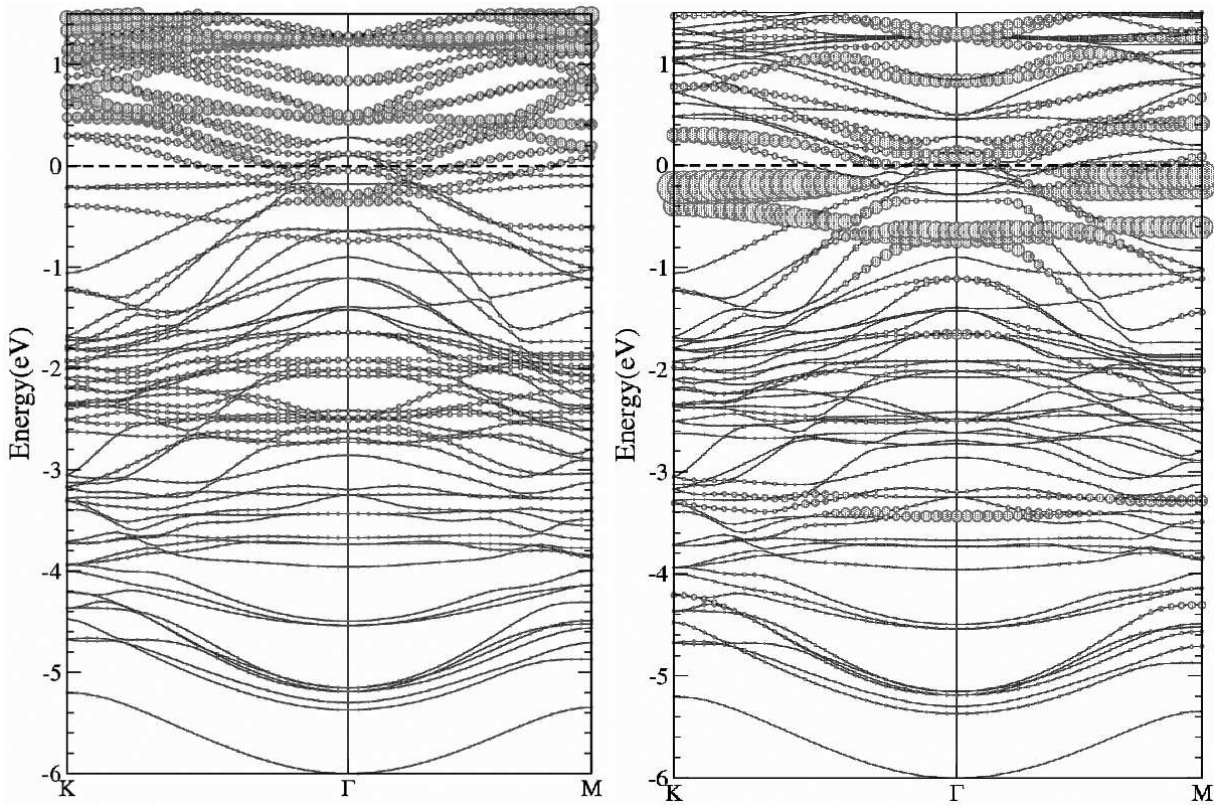


Fig. 7. Calculated dispersion curves for $Mn_{1/8}TiSe_2$, the circle diameter is proportional to the 3d zone filling by the titanium states (left panel) and manganese states (right panel). Under the Fermi level the 3d states of titanium with the orbital symmetry t_{2g} ($E_b=0.2$ eV) are Figked out in the vicinity of point Γ . The Mn 3d states take the whole range $M-\Gamma-K$ under the Fermi level, $\Delta E_b=0.5$ eV in width, and possess the mixed orbital $e_g - t_{2g}$ symmetry.

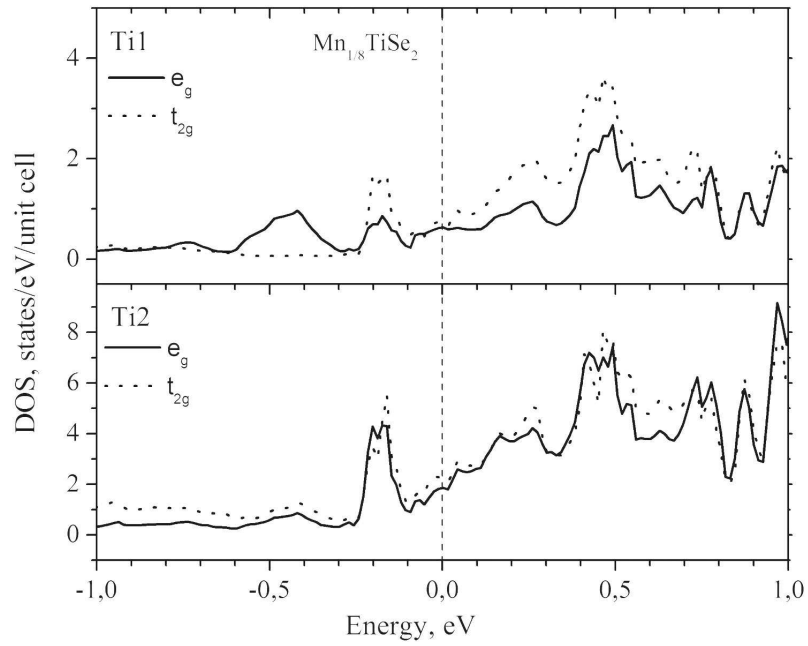


Fig. 8. Local density of states Ti 3d in two nonequivalent positions Ti1 and Ti2. For Ti1 there is observed polarization of electron density in the direction of the c axis. This polarization results in a relative increase of the e_g contribution of the states under the Fermi level in the energy range 0.3-0.6 eV.

